Pressure Tuning of the Spin-Orbit Coupled Ground State in Sr_{2}IrO_{4}

D. Haskel, G. Fabbris, Mikhail Zhernenkov, P. P. Kong, C. Q. Jin, G. Cao, and M. van Veenendaal

Phys. Rev. Lett. **109**, 027204 — Published 13 July 2012

DOI: 10.1103/PhysRevLett.109.027204

Pressure-tuning of spin-orbit coupled ground state in Sr_2IrO_4

D. Haskel[1*], G. Fabbris[1,2], Mikhail Zhernenkov[1], P. P. Kong[3], C. Jin[3], G. Cao[4], M. van Veenendaal[1,5]
[1] *Advanced Photon Source, Argonne National Laboratory, Argonne, IL 60439, USA*
[2] *Department of Physics, Washington University, St. Louis, MO 63130, USA*
[3] *Institute of Physics, Chinese Academy of Sciences, Beijing 100190, China*
[4] *Department of Physics and Astronomy and Center for Advanced Materials, University of Kentucky, Lexington, KY 40506*
[5] *Department of Physics, Northern Illinois University, De Kalb, IL 60115, USA*
(Received:)

X-ray absorption spectroscopy studies of the magnetic-insulating ground state of Sr_2IrO_4 at ambient pressure show a clear deviation from a strong spin-orbit (S-O) limit $J_{\rm eff} = \frac{1}{2}$ state, a result of local exchange interactions and a non-zero tetragonal crystal field mixing S-O split $J_{\rm eff} = \frac{1}{2}, \frac{3}{2}$ states. X-ray magnetic circular dichroism measurements in a diamond anvil cell show a magnetic transition at a pressure of $\sim$ 17 GPa where the "weak" ferromagnetic moment is quenched despite transport measurements showing insulating behavior to at least 40 GPa. The magnetic transition has implications for the origin of the insulating gap and the nature of exchange interactions in this S-O coupled system. The expectation value of the angular part of the S-O interaction, $\langle \mathbf{L} \cdot \mathbf{S} \rangle$, extrapolates to zero at $\sim$ 80-90 GPa where an increased bandwidth strongly mixes $J_{\rm eff} = \frac{1}{2}, \frac{3}{2}$ states and S-O interactions no longer dominate the electronic ground state of Sr_2IrO_4.

Iridate oxides continue to provide an attractive playground for testing fundamental interactions in correlated electron systems [1–16]. This is because a strong S-O interaction ($\sim$ 0.2-1 eV) acting on Iridium's $5d$ electrons competes with on-site Coulomb repulsion, intersite hopping and a crystal electric field (CEF) interaction arising from surrounding oxygen atoms in a nearly octahedral environment [1]. A strong S-O limit is usually assumed in Sr_2IrO_4 where the splitting of the CEF-derived t_{2g} manifold under the S-O interaction yields a half-filled, $J_{\rm eff} = \frac{1}{2}$ narrow band inducive to gap opening by Coulomb and/or exchange (magnetic) interactions [4]. The role of magnetic interactions in gap formation has remained a matter of debate with Sr_2IrO_4 alternatively labeled a Mott-Hubbard insulator (Coulomb and exchange interactions drive gap formation) [4], Mott insulator (Coulomb interactions alone drive gap formation) [5] and more recently a Slater insulator (magnetic ordering drives gap formation) [8]. In addition, the origin of "weak" ferromagnetism (WFM) in Sr_2IrO_4 has recently been addressed theoretically in terms of non-trivial exchange interactions accounting for the strong coupling of orbital magnetization to the lattice [6]. A magnetic phase diagram involving canted and collinear antiferromagnetic phases is predicted to exhibit strong sensitivity to the relative strength of S-O and non-cubic (tetragonal) CEF interactions acting on Ir $5d$ electrons [6].

In this *Letter* we show that a non-zero, x-ray magnetic circular dichroism signal at the Ir L_2 absorption edge, together with an experimental orbital-to-spin moment ratio $\langle L_z \rangle / \langle 2S_z \rangle = 1.05 \pm 0.14$, can be explained by accounting for exchange ($\sim$ 200 meV) and tetragonal crystal field ($\sim$ 75 meV) interactions modifying the electronic ground state away from the strong S-O limit $J_{\rm eff} = \frac{1}{2}$ state. Application of hydrostatic pressure induces a sharp magnetic phase transition at $\sim$ 17 GPa where the WFM of Sr_2IrO_4 suddenly vanishes with the material retaining insulating behavior to much higher pressures. A transition from canted to collinear antiferromagnetic (AFM) ordering driven by an increased tetragonal CEF under pressure is consistent with the magnetic and structural data, although a paramagnetic-insulating (PM-I) high-pressure phase cannot be ruled out. Additionally, the expectation value of $\langle \mathbf{L} \cdot \mathbf{S} \rangle$ decreases with pressure above $\sim$ 20 GPa and extrapolates to zero at about 80-90 GPa, a result of an increased bandwidth mixing $J_{\rm eff} = \frac{1}{2}, \frac{3}{2}$ states. The likely appearance of a single, metallic band at a pressure of $\sim$ 1 Mbar provides an exciting backdrop for searches of superconductivity [2]. Indeed unconventional superconductivity is found in $3d$ and $4d$ analog layered structures of $La_{2-x}(Ba,Sr)_xCuO_4$ [17] and Sr_2RuO_4 [18–20], where S-O interactions are weaker than in Sr_2IrO_4 [21].

In its ground state Sr_2IrO_4 is an insulating, "weak" ferromagnet with an ordering temperature T_N=240 K [5, 22, 23]. It displays anisotropic magnetization with a net moment of 0.06 (0.03) μ_B/Ir in a 0.5 T field applied in (out of) the IrO_2 planes, respectively [22]. We carried out x-ray absorption near edge structure (XANES) and magnetic circular dichroism (XMCD) measurements at ambient pressure to probe $\langle L_z \rangle$, $\langle S_z \rangle$, and $\langle \mathbf{L} \cdot \mathbf{S} \rangle$ in the ground state via sum rules analysis [24, 25]. Measurements were done on powder samples in a transmission geometry at beamline 4-ID-D of the Advanced Photon Source, Argonne National Laboratory. The helicity of a circularly polarized x-ray beam, generated with a 500 μm-thick diamond phase retarder [26], was modulated at

13.55 Hz and the related modulation in the absorption coefficient measured with a phase lock-in amplifier [27]. Measurements were repeated for opposite directions of a 0.8 T applied field (along and opposite the photon wave vector) to check for experimental artifacts.

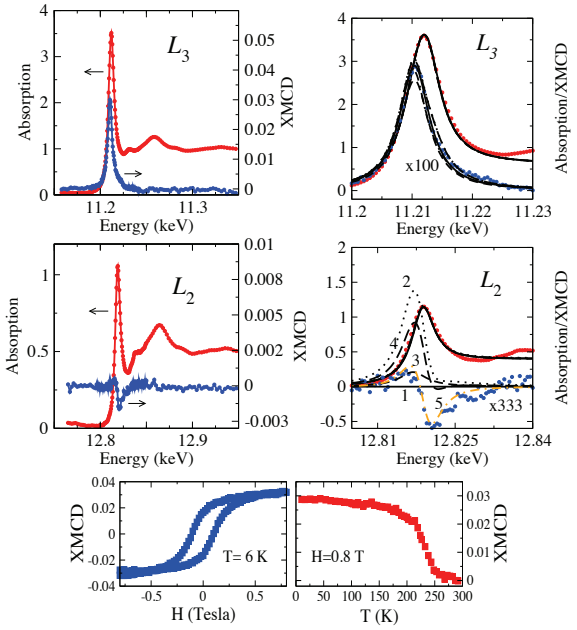

FIG. 1. (color online). (Top left) Ir $L_{2,3}$-edge XANES and XMCD data collected at T=6 K, H=0.8 T and ambient pressure. (Top right) CI calculations of XANES and XMCD intensities. All models (1-5) include S-O $\zeta_{5d} = 0.22$ eV and CEF $10Dq = 1.8$ eV interactions. Model 1 (solid) forces a pure $J_{\rm eff} = \frac{1}{2}$ state; Model 2 (dotted) adds an exchange field acting on the spin alone $H_{\rm exch} = \beta S_z$ with $\beta = 230$ meV; Model 3 (short dashed) adds a tetragonal CEF $\Delta = 75$ meV; Model 4 (long dashed) includes both $\Delta = 75$ meV and $H_{\rm exch} = \beta S_z$ with $\beta = 230$ meV; Model 5 (dotted-dashed) reproduces the data and includes $\Delta = 75$ meV and $H_{\rm exch} = \alpha L_z + \beta S_z$ with $\alpha = -22$ meV and $\beta = 230$ meV. (Bottom) Field- and temperature-dependent L_3-edge (E=11.2106 keV) XMCD peak intensity at ambient pressure.

Figure 1 (top left) shows normalized XANES ($\mu_c = [\mu^L + \mu^R]/2$) and XMCD ($\mu_m = \mu^L - \mu^R$) data at Ir $L_{2,3}$ absorption edges. The L_3-edge XMCD signal is ~ 20 times larger than the L_2 signal (these are equal and opposite in the absence of orbital magnetization). Sum rules analysis using n_h=5 for the number of $5d$ holes yields m_l= -0.023(3) μ_B/Ir and m_s=-0.022(3) μ_B/Ir [28] for the net orbital and spin moments, respectively, or a net magnetic moment $m = -(m_l + m_s)$= $0.045(4)\mu_B$/Ir. This is in close agreement with a random orientational average of magnetization data on single crystals ($0.05\mu_B$/Ir) [22]. Note that XMCD measures the *net* (ordered) FM moment which differs from the local moment (canted AFM). In the strong S-O coupling limit, however, $m_l/m_s = \langle L_z\rangle/2\langle S_z\rangle$ is a property of the local moment. The experimental value of $m_l/m_s = 1.05 \pm 0.14$ is roughly two times smaller than predicted for a purely ionic $J_{\rm eff} = \frac{1}{2}$ model [4]. In fact, the non-zero XMCD signal at the Ir L_2 edge indicates deviations from a $J_{\rm eff} = \frac{1}{2}$ ground state as corroborated by configuration interaction (CI) calculations detailed below. Note that the optical theorem and dispersion relations relate the XMCD signal to the imaginary and real parts of the x-ray resonant magnetic scattering (XRMS) amplitude, respectively, $\mu_m \propto f''_m(Q=0) \leftrightarrow f'_m(Q=0)$ (Q is scattering vector). The expected ratio of resonant magnetic scattering intensities at Ir $L_{2,3}$ edges in a diffraction experiment is therefore $I_{L_2}/I_{L_3} \propto |f_m(L_2)|^2/|f_m(L_3)|^2 \propto |\mu_m(L_2)/\mu_m(L_3)|^2 \approx 0.25\%$. This is in good agreement with the $< 1\%$ intensity ratio reported in the XRMS experiment of Ref. 5. Since the intermediate states probed in the second-order, XRMS process are the final states in the first-order XMCD process [29] it follows that the L_3/L_2 XRMS intensity ratio measured in Ref. 5 can be explained in terms of the values of the local moment ($\langle L_z\rangle$ and $\langle S_z\rangle$) without the need to invoke the phase sensitivity of the resonant scattering process [5, 7].

The S-O coupled ground state is also reflected in the measurement of the branching ratio, BR=I_{L_3}/I_{L_2}, where $I_{L_{2,3}}$ is the integrated intensity of the resonantly enhanced absorption cross section near threshold ("white line") in the isotropic (XANES) spectrum of a particular S-O split edge. BR is directly related to the ground state value of $\langle \mathbf{L}\cdot\mathbf{S}\rangle$ of the empty $5d$ states through BR=$(2+r)/(1-r)$, with $r = \langle \mathbf{L}\cdot\mathbf{S}\rangle/\langle n_h\rangle$ [25]. We measured BR=4.1(2), which differs significantly from the statistical BR=2 in the absence of orbital magnetization in the $5d$ states. With $n_h = 5$, we obtain $\langle \mathbf{L}\cdot\mathbf{S}\rangle = 2.1(1)\hbar^2$. Since $\langle \mathbf{L}\cdot\mathbf{S}\rangle$ is a property of the local moment (independent of magnetic ordering), it is mostly determined by the Ir valence ($5d$ occupation), the CEF, and the S-O coupling interaction acting on $5d$ electrons [30]. Hence, its value is expected to be similar for all $Ir^{4+}O_6$ units with (nearly) O_h octahedral symmetry [9]. Note that since XANES probes all empty $5d$ states, the measured $\langle \mathbf{L}\cdot\mathbf{S}\rangle$ includes contributions from the single hole in the $J_{\rm eff} = \frac{1}{2}$ state ($\langle \mathbf{L}\cdot\mathbf{S}\rangle = 1$) [7] and 4 holes in the e_g-derived states [9] ($\langle \mathbf{L}\cdot\mathbf{S}\rangle \approx 4 \times 3\zeta_{5d}/10Dq = 1.47$, with S-O $\zeta_{5d} = 0.22$ eV and octahedral CEF $10Dq$=1.8 eV obtained from CI calculations). Summing over the occupied $J_{\rm eff} = \frac{1}{2}, \frac{3}{2}$ states gives the same magnitude of $\langle \mathbf{L}\cdot\mathbf{S}\rangle$, albeit with opposite sign.

Results from CI calculations [31] (see supplemental material [32] for details) are shown in Fig. 1 (top right). All models (1-5) include (best fit) $\zeta_{5d} = 0.22$ eV and $10Dq$=1.8 eV interactions. While the L_3-edge calculations reproduce the data rather well in all models, the small L_2-edge XMCD signal yields strong sensitivity to the details of the model. Model 1 forces a pure $J_{\rm eff} = \frac{1}{2}$ state. An infinitesimal exchange field was added to lift the degeneracy of $m_{j_{\rm eff}} = (1/2, -1/2)$ components giving rise to XMCD (magnetic ordering). The model re-

turns $L_z, S_z, (L_z/2S_z)$, and BR values of $\frac{2}{3}\mu_B$, $\frac{1}{6}\mu_B$, 2, and 4.3, respectively, and equal hole occupations for $|xy\rangle, |yz\rangle, |zx\rangle$ components of the ground state wavefunction, as expected [4]. Model 1, however, fails to reproduce the data since it gives zero L_2 edge XMCD intensity. Succesfull modeling of the data (model 5) requires inclusion of exchange interactions acting both on spin and orbital moments ($H_{\rm exch} = \alpha L_z + \beta S_z$ with $\alpha = -22$ meV and $\beta = 230$ meV) and a tetragonal crystal field $\Delta = 75$ meV (octahedron elongated along the c-axis [23]). Note that both exchange and tetragonal CEF interactions mix $J_{\rm eff} = \frac{1}{2}, \frac{3}{2}$ states and determine the (unequal) final hole occupations (0.22, 0.42, 0.42) for the $(|xy\rangle, |yz\rangle, |zx\rangle)$ components of the ground state wavefunction, respectively [33]. Model 5 returns $L_z, S_z, (L_z/2S_z)$, and BR values of 0.63 μ_B, 0.31 μ_B, 1.01, and 4.26, respectively, in good agreement with experiment. While fitted values of $\Delta = 75$ meV and $\zeta_{5d} = 220$ meV satisfy the $\Delta < \zeta_{5d}/2$ relation theoretically predicted for an in-plane WFM structure, as observed in experiments at ambient pressure [5, 6], the mixing of $J_{\rm eff}$ states necessary to reproduce the XMCD data indicates that Sr_2IrO_4 cannot be fully described within the strong S-O limit.

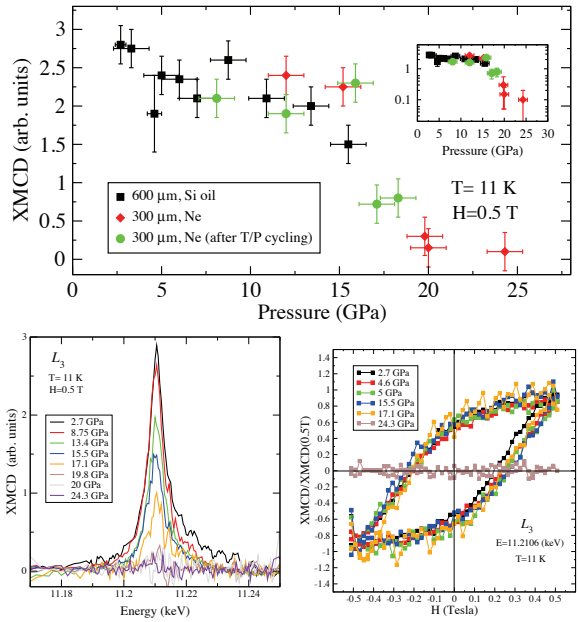

FIG. 2. (color online). (Top) Pressure-dependence of Ir L_3-edge XMCD signal. Inset displays the data in log scale to highlight the sharpness of the magnetic transition. (Bottom) Raw XMCD data (left), and field-dependent XMCD signal (right) normalized to its value at 0.5 T, under applied pressure.

We now turn to the magnetic and transport measurements at high pressure. A membrane-driven, Copper-Beryllium (CuBe) diamond anvil cell (DAC) was used for XMCD measurements at the Ir L_3-edge (T=11 K) [34]. Pressure was calibrated *in-situ* at low temperatures using the Ruby fluorescence method [35]. The XMCD experiment was done on a powder sample using a transmission geometry. Resistance (four probe) measurements were carried out in a CuBe DAC on a single crystal, using slim Au wires as electrodes and soft hexagonal BN fine powder as pressure medium as described in Ref. 36. Further details on experimental conditions can be found in the supplemental material [32].

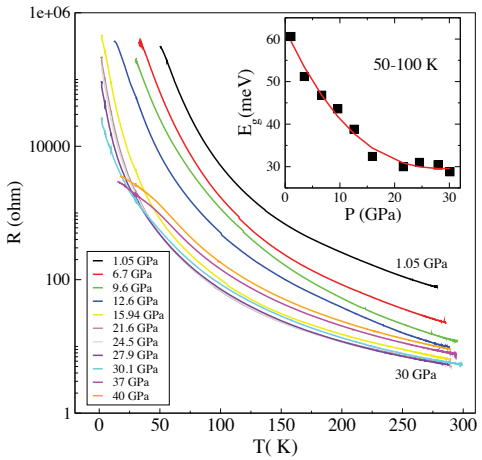

FIG. 3. (color online). Resistance versus temperature at various pressures from four-probe measurements in the DAC (main panel). Estimates of the insulating gap (inset) are obtained using lnR$\propto \frac{E_g}{2k_BT}$ in the 50-100 K range.

Figure 2 shows pressure-dependent XMCD data obtained in three independent experimental runs. A clear magnetic transition is observed at P$\sim$ 17 GPa, the "weak" ferromagnetic component vanishing at 20 GPa. The transition is reversible, the XMCD signal recovered after pressure release from 24 GPa to 8 GPa concomitant with an 11 K$\rightarrow$ 300 K $\rightarrow$ 11 K temperature cycle. A vanishing XMCD signal at 20 GPa, together with a collapse of hysteresis and remanent magnetization in field-dependent XMCD data (Fig. 2) would be consistent with a transition into either a paramagnetic (PM) state or a collinear AFM state (as discussed below, a constant BR to at least 20 GPa indicates that the local, S-O coupled moment remains unchanged through the magnetic transition). We first address the possibility of a high-pressure PM state. Figure 3 shows that Sr_2IrO_4 remains an insulator to at least 40 GPa; i.e., far above the pressure range where the collapse of WFM ordering is observed. If PM, the disparate difference in pressure (energy) scale associated with the magnetic and I-M transition would clearly indicate that the electronic gap is not driven by the onset of magnetic ordering, as recently claimed [8] but rather by Coulomb interactions within a $J_{\rm eff} = \frac{1}{2}$ narrow band; i.e., Sr_2IrO_4 would classify as a Mott or Mott-Hubbard insulator and not a Slater insulator [8]. Note that the ambient pressure value of the energy gap derived from the resistance measurements is in excellent

agreement with previous resistivity measurements [4] and in reasonable agreement with the 100 meV gap reported from optical conductivity measurements at 100 K [4].

Since the WFM ordering (canted AFM) at ambient pressure is driven by $\sim 11^\circ$ rotations of IrO_6 octahedra around the c-axis through the Dzyaloshinskii-Moriya (DM) interaction [6,23], disappearance of these rotations under pressure, while unlikely, may lead to a collinear AFM phase. Even more interesting is the theoretical prediction of a spin-flop transition from in-plane WFM to c-axis collinear AFM at a critical value $\Delta \geqslant \zeta_{5d}/2$ [6]. We probed for structural changes at high pressure using x-ray diffraction. Experiments were conducted at HP-CAT beamline 16-BM-D of the Advanced Photon Source using a membrane-driven symmetric DAC, He gas as pressure medium and Ruby spheres for in-situ pressure calibration. Measurements were carried out at T= 11 K up to 25 GPa. Further details are given in the supplemental material [32]. Lattice parameters were refined within the $I4_1/acd$ tetragonal space group [23]. No discontinuities in lattice parameters or signatures of a structural phase transition are observed in this pressure range, indicating that the rather sharp magnetic transition is not driven by a concomitant structural transition. However, the a-axis contracts at a faster rate than the c-axis ($\frac{\Delta a/a_0}{\Delta P}$=-0.146(5)%/GPa; $\frac{\Delta c/c_0}{\Delta P}$=-0.125(5)%/GPa). A gradual disappearance of IrO_6 rotations under pressure would have likely resulted in a faster c-axis compression, contrary to observation. On the other hand, the faster in-plane compression may be indicative of an increased (positive) tetragonal distortion with pressure. Our CI calculations together with results in Ref. 6 indicate that Sr_2IrO_4 is not far from the critical $\Delta = \zeta_{5d}/2$ value needed to induce a spin-flop transition into a collinear Néel state along the c-axis. An increasing tetragonal crystal field with pressure may provide a natural explanation for the disappearance of WFM ordering without a concomitant I-M transition- localized moments would tend to order magnetically at low temperature due to strong local exchange interactions $H_{ex} \gg k_B T$ [37]- although a high-pressure, PM-insulating phase cannot be ruled out.

Since pressure increases bandwidth (hopping) relative to Coulomb and S-O interactions it is expected that high enough pressures will lead to strong mixing of S-O split $J_{\rm eff} = \frac{1}{2}, \frac{3}{2}$ bands and render Sr_2IrO_4 a "normal" metal where S-O physics no longer dominates. Support for this comes from measurements of the BR at T=300 K carried out at beamline 20-BM of the Advanced Photon Source using 180 μm diamond culets and Neon gas as pressure medium. Figure 4 shows the white line intensity at the L_3 edge decreasing with pressure while the opposite is observed at the L_2 edge indicating a reduction in BR (i.e. a reduction in $\langle \mathbf{L} \cdot \mathbf{S} \rangle$). The effect is reversible upon pressure release. While the BR is nearly constant to 25 GPa (note this is above the collapse of WFM ordering), it decreases rapidly above this pressure, extrapolating to the statistical BR=2 ($\langle \mathbf{L} \cdot \mathbf{S} \rangle$=0) at P$\approx$ 90 GPa. Note that a change in (cubic) CEF with pressure, estimated to increase by $\sim$ 50% (1.8 to 2.7 eV) at 70 GPa based on a linear extrapolation of the high-pressure XRD data [38], can only account for a small fraction of the observed reduction in BR. An increased tetragonal distortion would reduce the BR further (BR=3.45 for Δ=200 meV) [38], but again not enough to account for the experimental observation.

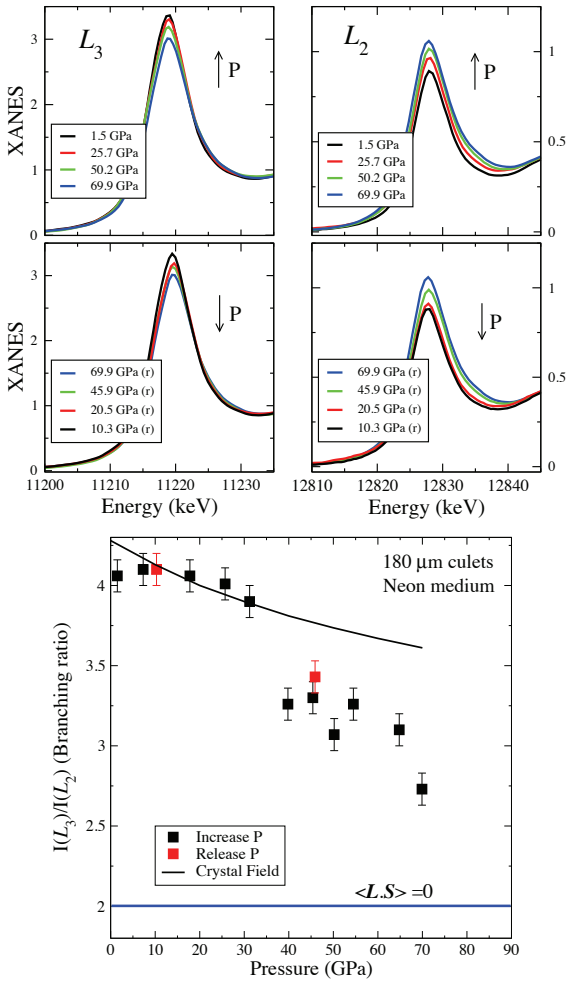

FIG. 4. (color online). Ir $L_{2,3}$ XANES data at T=300 K as a function of pressure to 70 GPa (top), together with the derived branching ratio (bottom).

We conclude that the fast reduction in BR must originate in bandwidth-driven mixing of $J_{\rm eff} = \frac{1}{2}, \frac{3}{2}$ states and related quenching of orbital angular momentum in $5d$ states. Since the separation between $J_{\rm eff}$ states, $\zeta_{5d} \sim 0.22$ eV, is much larger than the insulating gap ($\sim$ 30 meV at 30 GPa, Fig. 3) a bandwidth-driven I-M transition would take place before $J_{\rm eff}$ states are fully mixed by band effects ($\sim$ 100 GPa= 1 Mbar). It ap-

pears that the high-pressure regime above 1 Mbar could offer interesting opportunities for searches of superconductivity [2] as the electronic properties of Sr_2IrO_4 move closer to those found in $3d$ cuprates and $4d$ Ruthenates displaying weaker S-O interactions.

We would like to thank B.J. Kim for illuminating discussions. Work at Argonne and NIU is supported by the U.S. Department of Energy, Office of Science, under contract Nos. DE-AC02-06CH11357 and DE-FG02-03ER46097, respectively. Work at UKY was supported by NSF through grants DMR-0856234 and EPS-0814194. Work at IOPCAS was supported by NSF&MOST of China through research projects. We thank Steve Heald, Mali Subramanian, Chengjun Sun, Changyong Park, Curtis Kenny-Benson and Dmitry Popov for their kind support at 20-BM and 16-BM. We also thank GSE-CARS for use of their DAC gas loading facility.

* haskel@aps.anl.gov

[1] D. Pesin and L. Balents, Nature Phys. **6**, 376 (2010).
[2] F. Wang and T. Senthil, Phys. Rev. Lett. **106**, 136402 (2011).
[3] A. Shitade *et al.*, Phys. Rev. Lett. **102**, 256403 (2009).
[4] B. J. Kim *et al.*, Phys. Rev. Lett. **101**, 076402 (2008).
[5] B.J. Kim, H. Ohsumi, T. Komesu, S. Sakai, T. Morita, H. Takagi, T. Arima, Science **323**, 1329 (2009).
[6] G. Jackeli and G. Khaliullin, Phys. Rev. Lett. **102**, 017205 (2009)
[7] L. C. Chapon and S. W. Lovesey, J. Phys.: Condens. Matter **23**, 252201 (2011).
[8] R. Arita, J. Kunes, A. V. Kozhevnikov, A. G. Eguiluz, M. Imada, Phys. Rev. Lett. **108**, 086403 (2012).
[9] Ma. Angeles Laguna-Marco, D. Haskel, N. Souza-Neto, J. Lang, V. Krishnamurthy, S. Chikara, G. Cao, M. van Veenendaal, Phys. Rev. Lett. **105**, 216407 (2010).
[10] L. J. P. Ament, G. Khaliullin, J. van der Brink, Phys. Rev. B **84**, 020403 (2011).
[11] X. Liu, W. G. Yin, W. Ku, A. Tsvelik, Y-J. Kim, H. Gretarsson, Y. Simgh, P. Gegenwart, J. P. Hill, Phys. Rev. B **83**, 220403 (2011).
[12] H. Okabe, N. Takeshita, M. Isobe, E. Takayama-Muromachi, T. Muranaka, J. Akimitsu, Phys. Rev. B **84**, 115127 (2011).
[13] J. G. Cheng, J. S. Zhou, J. B. Goodenough, Phys. Rev. B **82**, 132103 (2010).
[14] S. Zhao, J. M. Mackie, D. E. MacLaughlin, O. O. Bernal, J. J. Ishikawa, Y. Ohta and S. Nakatsuji, Phys. Rev. B **83**, 180402 (2011).
[15] O. B. Korneta, S. Chikara, S. Parkin, L. E. DeLong, P. Schlottmann, G. Cao, Phys. Rev. B **81**, 045101 (2010).
[16] G. Cao, J. Boliver, S. McCall, J. E. Crow, R. P. Guertin, Phys. Rev. B **57**, R11039 (1998).
[17] J. G. Bednorz and K. A. Müller, Z. Phys. B-Condensed Matter **64**, 189 (1986).
[18] Y. Maeno *et al.*, Nature **372**, 532 (1994).
[19] G. M. Luke *et al.*, Nature **394**, 558 (1998).
[20] K.D. Nelson, Z. Q. Mao, Y. Maeno, Y. Liu, Science **306**, 1151 (2004).
[21] M. W. Haverkort, I. S. Elfimov, L. H. Tjeng, G. A. Sawatzy, A. Damascelli, Phys. Rev. Lett. **101**, 026406 (2008).
[22] M. Ge, T. F. Qi, O. B. Korneta, D. E. De Long, P. Schlottmann, W. P. Crummett, G. Cao, Phys. Rev. B **84**, 100402 (2011).
[23] M. K. Crawford, M. A. Subramanian, R. L. Harlow, J. A. Fernandez-Baca, Z. R. Wang, D. C. Johnston, Phys. Rev. B **49**, 9198 (1994).
[24] B. T. Thole, P. Carra, F. Sette, G. van der Laan, Phys. Rev. Lett. **68**, 1943 (1992); P. Carra, B. T. Thole, M. Altarelli, X. Wang, Phys. Rev. Lett. **70**, 694 (1993); C. T. Chen, Y. U. Idzerda, H. J Lin, N. V. Smith, G. Meigs, E. Chaban, G. H. Ho, E. Pellegrin, F. sette, Phys. Rev. Lett. **75**, 152 (1995).
[25] G. van der Laan and B. T. Thole, Phys. Rev. Lett. **60**, 1977 (1988). Note that we adopted a definition where $\langle \mathbf{L} \cdot \mathbf{S} \rangle$ refers to the empty (hole) states while van der Laan and Thole refer to occupied states resulting in a sign reversal in the definition of r.
[26] K. Hirano *et al.*, Jpn. J. Appl. Phys. **30**, L407 (1991); J. C. Lang and G. Srajer, Rev. Sci. Instrum. **66**, 1540 (1995).
[27] M. Suzuki *et al.*, Jpn. J. Appl. Phys. **37**, L1488 (1998).
[28] The spin sum rule requires knowledge of $\langle T_z \rangle$ where T_z is the magnetic dipole operator. We used $\langle T_z \rangle / \langle S_z \rangle = 0.18$ obtained from configuration interaction calculations. Neglecting T_z yields $m_s = 0.0375\ \mu_B$/Ir and $\langle L_z \rangle / 2 \langle S_z \rangle = 0.61$.
[29] S. W. Lovesey and S.P. Collins in *X-ray Scattering and Absorption by Magnetic Materials*, Clarendon Press, Oxford 1996.
[30] Exchange interactions lift the degeneracy of $m_{j_{\rm eff}} = 1/2, -1/2$ components of $J_{\rm eff} = \frac{1}{2}$ states, rendering them inequivalent. CI calculations show that exchange interactions have a weaker effect on the BR.
[31] B. T. Thole *et al.*, Phys. Rev. B **32**, 5197 (1985).
[32] *See supplemental material at [url will be inserted by publisher] for details*
[33] Note that exchange interactions yield an enhanced occupation of $|xy\rangle$ versus $(|yz\rangle, |zx\rangle)$ components at ambient pressure, despite the presence of a (small) positive tetragonal crystal field.
[34] D. Haskel *et al.*, High Pressure Research **28**, 185 (2008); D. Haskel *et al.*, Rev. Sci. Instrum. **78**, 083904 (2007).
[35] K. Syassen, High Press. Res. **28**, 75 (2008).
[36] S. J. Zhang *et al.*, Europhys. Lett. **88**, 47008 (2009).
[37] J. Kim *et al.*, Phys. Rev. Lett. **108**, 177003 (2012).
[38] $10Dq$ is adjusted in CI calculations using the r^{-5} power law, r the Ir-O distance [W. A. Harrison in Electronic Structure and Properties of Solids (Dover, New York, 1989)]. A linear extrapolation of XRD data to 70 GPa gives a $\sim$ 10% change in Ir-O distance, increasing the CEF by $\sim$ 50%. Assuming IrO_6 rotations are unchanged the tetragonal distortion, $(r_a - r_c)/(r_a + r_c)$ with $r_{a,c}$ in-plane and out-of-plane Ir-O distances, increases from 1.9% at P=1 bar to a linearly extrapolated 2.7% at 70 GPa.